High order mesh untangling for complex curved geometries

Cecile Dobrzynski, Ghina El Jannoun

High order mesh untangling for complex curved geometries

C. Dobrzynski, G. Jannoun

RESEARCH REPORT
N° 9120
November 2017
Project-Teams Cardamom

ISSN 0249-6399 ISRN INRIA/RR--9120--FR+ENG

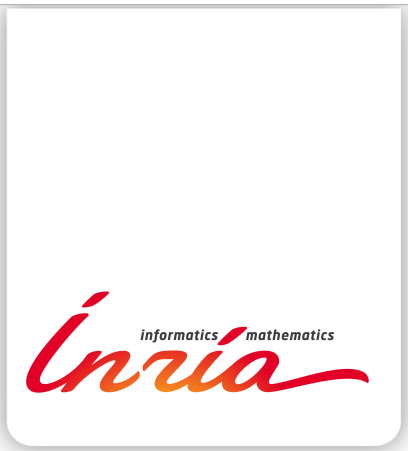

High order mesh untangling for complex curved geometries

C. Dobrzynski [*] [†], G. Jannoun [†]

Équipes-Projets Cardamom

Rapport de recherche n° 9120 — November 2017 — 17 pages

Résumé : Dans ce document, nous proposons une nouvelle approche pour construire des maillages simpliciaux courbes représentant exactement une frontière définie par des patches de Bézier quadratiques. Cette méthode est composée de deux parties distinctes : d'une part une analogie élastique pour détordre les éléments de volumes et d'autre part une méthode d'optimisation topologique locale pour rendre valide les éléments surfaciques. Partant d'un maillage linéaire avec une frontière courbe quadratique, la première étape de notre algorithme consiste à détordre les éléments de surface. Dans cette phase, le problème est écrit comme un problème d'optimisation non contraint grâce à l'utilisation d'une méthode log-barrier. La seconde étape de l'algorithme propage la courbure de la surface au volume en considérant le maillage comme un solide élastique. Des exemples en deux et trois dimensions sont fournis pour valider la méthode proposée.

Mots-clés : maillage d'ordre élevé, génération de maillage courbe, optimisation topologique.

[*] IMB, Bordeaux INP, 351 cours de la Libération, 33405 Talence Cedex
[†] Cardamom team, Inria-Bordeaux, 200 avenue de la vieille Tour, 33405 Talence Cedex

RESEARCH CENTRE
BORDEAUX – SUD-OUEST

200 avenue de la Vieille Tour
33405 Talence Cedex

High order mesh untangling for complex curved geometries

Abstract: We propose a new approach for constructing and untangling curved simplicial meshes that fit exactly to a geometrical boundary defined using quadratic Bézier patches. The method comprises two main ingredients: a linear elasticity analogy for untangling volume elements on the one hand and a local topological optimization for resolving invalid surface elements on the other hand.
Starting from a linear mesh with a quadratic curved boundary, the first step of the algorithm consists in untangling surface mesh elements. In this phase, the problem is cast as a constrained optimization one whereby the worst element's quality is improved iteratively under the constraint of maintaining valid neighboring elements. The problem is then reformulated as an unconstrained optimization through the use of a log-barrier method. The second step of the algorithm involves propagating the curvature to the volume of the domain via a linear elasticity analogy resulting in a valid volume mesh. Finally, two and three dimensional numerical examples are provided to validate the proposed approach.

Key-words: high order mesh, curved mesh generation, local topological optimization.

1 Introduction

Over the last decade, there has been an increased interest in the development of high order numerical schemes in the view of capturing with a high fidelity the solution of unsteady CFD problems on complex geometries. High convergence rates of these numerical method were noted in the presence of high order meshes that describe more accurately the computational domain. However, the generation of valid 3D high order meshes still poses technical challenges especially in the presence of boundary layers and non-convex domains. Starting from an initial mesh with curved boundary and linear internal elements, the curvature needs to be propagated onto the volume in the view of generating a valid mesh. Several methods were proposed in the literature for untangling the invalid elements that can result from the curving of the mesh edges at the level of the geometry's curved boundary. The approaches include performing some local modifications on the volume mesh [1, 2, 3, 4, 5], propagating the curvature inside the domain with smoothing schemes like the Laplacian, linear elasticity smoothing [6, 7], non linear elasticity smoothing [8] and through quality optimization and distortion minimization algorithms [9, 10].

This paper aims at presenting a novel automatic and robust approach for constructing, in 2D and 3D, curved simplicial meshes that fit exactly to a geometrical boundary defined using quadratic Bézier patches. We develop a hybrid method comprising two main ingredients : a linear elasticity analogy, developed in [5], for untangling volume elements on the one hand and a local topological optimization for resolving invalid surface elements on the other hand.

The remainder of this paper is structured as follows. We provide, in section 2, some basic definitions on Bézier approximations, followed, in section 3, by the derivation of the validity criteria for high order meshes. Sections 4 and 5 describe respectively the first and second components of the hybrid algorithm. Finally, some numerical validations in two and three dimensional spaces are discussed in section 6.

2 Overview on the topology of high Order Bézier representation

In this section, we provide an overview on Bézier parametrizations for high order tetrahedral elements that will be adopted throughout the paper.

We consider a simplex $K \subset \mathbb{R}^d$, i.e. the convex hull of $d+1$ independent points $\{P_1, \ldots, P_{d+1}\}$, such that :

$$\text{Vol}(K) = \frac{1}{d+1} \left| \det(\overrightarrow{P_{d+1}P_1}, \ldots, \overrightarrow{P_{d+1}P_d}) \right| > 0. \tag{1}$$

Without loss of generality, we assume that the vertices are ordered in such a way to ensure the positivity of $\det(\overrightarrow{P_{d+1}P_1}, \ldots, \overrightarrow{P_{d+1}P_d})$.

We let $\mathcal{I}$ be an n-tuple of multi-indices α, $\alpha = (\alpha_1, \ldots, \alpha_{d+1})$ where $(\alpha_i \in \mathbb{N})$ and whose length is given by $|\alpha| = \sum_{i=1}^{d+1} \alpha_j$. We set for $\mathbf{x} = (x_1, \ldots, x_{d+1})$,

$$\mathbf{x}^\alpha := x_1^{\alpha_1} x_2^{\alpha_2} \ldots x_{d+1}^{\alpha_{d+1}}.$$

Then the Bézier polynomial, for any $M \in \mathbb{R}^d$, is given by :

$$B_\alpha^n(M) := c(\alpha) \Pi_{i=1}^{d+1} \lambda_i(M)^{\alpha_i}\,, \tag{2}$$

where $c(\alpha)$ are the coefficient of x^α in the development

$$\big(\sum_{i=1}^{d+1} x_i\big)^n = \sum_{\alpha, |\alpha|=n} c(\alpha) \mathbf{x}^\alpha\,,$$

and $\lambda_1(M), \ldots, \lambda_{d+1}(M)$ are the barycentric coordinates of M :

$$\lambda_i(M) = \frac{\det\left(\overrightarrow{P_jP_1}, \ldots, \widehat{\overrightarrow{P_jP_i}}, \ldots, \overrightarrow{P_jP_d}\right)}{\det(\overrightarrow{P_jP_1}, \ldots, \overrightarrow{P_jP_d})} \tag{3a}$$

with,

$$\widehat{\overrightarrow{P_jP_i}} = \overrightarrow{P_jM}. \tag{3b}$$

The family of Bézier polynomials defines a basis of $\mathbb{P}_n(x_1, \ldots, x_{d+1})$ with dimension $N_d^n = \sum_{p=0}^{n} \binom{p+d-1}{p}$ and satisfying, for any $\alpha, |\alpha| = n$ and $M \in K$,

$$B_\alpha^n(M) \geq 0 \qquad \text{and} \qquad \sum_{\alpha, |\alpha|=n} B_\alpha^n(M) = 1. \tag{4}$$

We recall that

$$\binom{|\alpha|}{\alpha} = \frac{|\alpha|!}{\Pi_{i=1}^{d+1} \alpha_i!}.$$

Finally, given a family of control points $\mathcal{C} = \{C_\alpha \in \mathbb{R}^p, \alpha \in \mathcal{I}\}$, we approximate a function ψ defined on K with values in $\mathbb{R}^p$, $p > 0$, by

$$\psi(M) \approx \sum_{\alpha, \alpha \in \mathcal{I}} C_\alpha \varphi_\alpha^n \,,$$

where φ_α^n stands for a Bézier polynomial. Clearly the control parameters should be selected carefully to have a good approximation. Bearing in mind the previously mentioned notations and definitions, we obtain the following property :

Property 2.1 (Convex hull property)**.** *For any $M \in K$, if relations* (4) *are satisfied then $\psi(M)$ lies in the convex hull of $\mathcal{P}$.*

Property 2.2. *For a segment element K, the tangent vectors to the curve $\psi(M)$ are in the same direction as the first and last control polygon spans, respectively.*

We note that this property is not true for any order Lagrange interpolation because the basis functions are not always positive. It is only satisfied for $n = 1$ where the Lagrange interpolation polynomials coincide with the Bézier polynomials.

3 Curved element validity criteria

We aim in this section at providing a review on the validity criteria for high order elements. We follow the lines in [5] for the definition of the validity criteria. The latter definition was derived by exploiting the Jacobian properties of the mapping Ψ of a reference simplex K in the linear mesh onto a curved simplex $\hat{K}$ shown in figure 1. In the following section, in the view of untangling a given curved mesh, we derive constraints on the positions of the mesh nodes and control points that are necessary to ensure the validity of the curved elements.

We start by expressing the Jacobian of the mapping using the barycentric coordinates :

$$\begin{aligned} J \;=\; & \left(\det(\vec{a}_{16}, \vec{a}_{34}) + \det(\vec{a}_{24}, \vec{a}_{26})\right) \Lambda_1\Lambda_2 + \det(\vec{a}_{16}, \vec{a}_{26})\Lambda_1^2 \\ & - \left(\det(\vec{a}_{16}, \vec{a}_{54}) + \det(\vec{a}_{56}, \vec{a}_{26})\right) \Lambda_1\Lambda_3 + \det(\vec{a}_{24}, \vec{a}_{34})\Lambda_2^2 \\ & - \left(\det(\vec{a}_{24}, \vec{a}_{54}) + \det(\vec{a}_{56}, \vec{a}_{34})\right) \Lambda_3\Lambda_2 + \det(\vec{a}_{56}, \vec{a}_{54})\Lambda_3^2 \end{aligned}$$

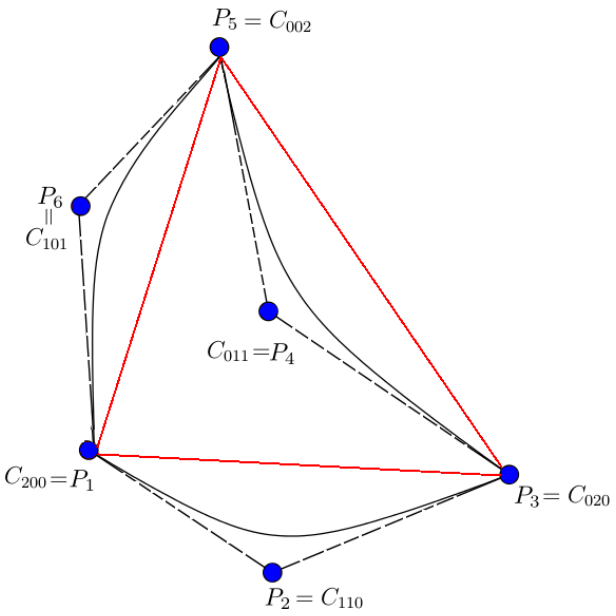

FIGURE 1 – Mapping of a simplex (red) onto quadratic Bézier curves (black).

where $\vec{a}_{ij} = 2(P_i - P_j)$. The positivity of the transformation's Jacobian will thus be conveyed into the following validity conditions :

$$\begin{array}{lll} \det(\vec{a}_{16}, \vec{a}_{26}) \geq 0 & \det(\vec{a}_{24}, \vec{a}_{34}) \geq 0 & \det(\vec{a}_{56}, \vec{a}_{54}) \geq 0 \\ \det(\vec{a}_{16}, \vec{a}_{34}) + \det(\vec{a}_{24}, \vec{a}_{26}) \geq 0 & \det(\vec{a}_{54}, \vec{a}_{16}) + \det(\vec{a}_{26}, \vec{a}_{56}) \geq 0 & \\ \det(\vec{a}_{54}, \vec{a}_{24}) + \det(\vec{a}_{34}, \vec{a}_{56}) \geq 0 & & \end{array} \quad (5)$$

with a strict positivity requirement on at least one of them. For more details on the derivation and interpretation of the validity constraints, the reader is referred to [5].

Remark 3.1. *The first three validity conditions can be interpreted as positivity constraints on the areas of triangles $P_1P_2P_6$, $P_2P_3P_4$ and $P_6P_4P_5$.*

Remark 3.2. *The validity conditions are generalized in the three dimensional case to verifying the positivity of the sub-volumes of the tetrahedron under consideration.*

Starting from an invalid linear mesh with a curved boundary, the novel technique proposed in this paper aims at propagating the curvature onto the domain in the view of untangling the invalid elements and improving the quality of the mesh elements. The method proceeds by local topological transformations inside patches constructed around invalid elements. It has first been developed to generate two-dimensional valid meshes then generalized to deal with three-dimensional surface elements. The new formulation consists in repairing invalid elements resulting from curving the surface boundary to fit the geometrical boundary while conserving its exact representation. This is achieved by limiting the distortion arising from the displacement of the boundary nodes and control points. In other words, the points defined on the faces of the initial mesh can only move along the surfaces of the geometrical model whereas the ones positioned on model geometrical edges are allowed to move only along these edges. In order to track these points, we define the ridges, or geometrical edges, as the edges delimiting the sharp intersection of two geometrical surfaces in the model. Practically, ridges are determined from the initial mesh based on a threshold value on the dihedral angle between two adjacent surface triangles [12].

4 Surface untangling procedure via local topological optimization

This section presents the main steps for the mesh untangling technique applied on surface mesh elements. The problem is cast as a constrained optimization one whereby the worst element's quality is improved iteratively under the constraint of maintaining the validity of the neighboring elements. To this end, the problem is reformulated as an unconstrained optimization through the use of a log-barrier method. We start this section by illustrating on the construction of the local patches around invalid elements. The constrained optimization problem aiming at improving the patch elements' validity is then defined in subsection 3. Finally, the unconstrained problem is deduced and solved to determine the optimal configuration of the nodes and control points resulting in a valid curved patch.

4.1 Patch construction around an invalid element

The optimization approach considers each invalid element at a time and improves the validity of a local patch around it by relocating the set of free nodes and control points contained in that patch. The construction of a first level in the patch is performed around a node of the invalid element by considering the elements sharing this node. The second level in the patch will then be constituted of the direct neighbors of the first level elements. Figure 2 depicts a patch constructed around a generic invalid element. The nodes and control points on the boundary of the patch are fixed and the ones that are on the curved

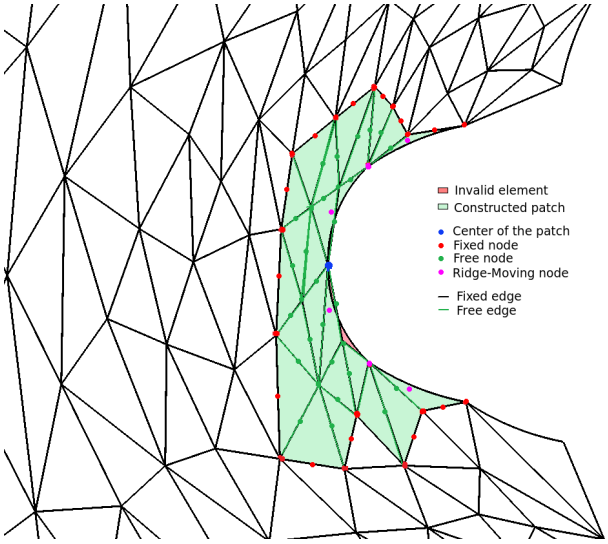

FIGURE 2 – Patch construction around a node of an invalid element.

domain boundary are allowed to slide along that curve while respecting the curvature. Finally, all inner nodes and control points are allowed to move freely inside the domain.

When a boundary layer is constructed at the geometry's curved boundary, a special treatment is considered especially when the invalid element's curved edge intersects several mesh elements. A graphical illustration of such a situation is presented in figure 3. In that case, considering the first degree neighbors is not enough for untangling. Therefore, a new ingredient is proposed for the patch construction. It involves adding to the first level elements in the patch all the elements contained in the Bézier polygon associated with the invalid element under consideration. The second level will then be formed as described above. In the three dimensional case, the method will only be applied to untangle triangles lying on the surface of the domain. Hence the patch will also be limited to the triangles on the surface neighboring a node of

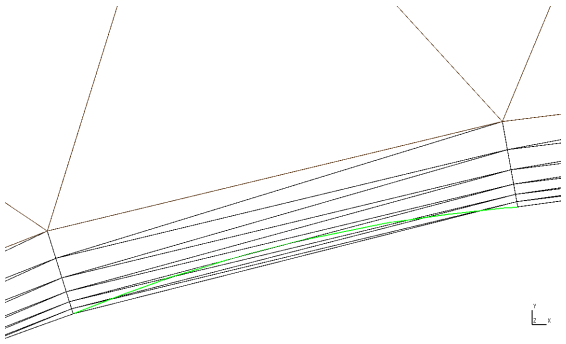

FIGURE 3 – Invalid element intersecting several mesh elements.

the invalid triangle under consideration. In this case, the nodes can move freely along the surface whereas the ones lying on a ridge can slide over that ridge.

4.2 Validity improvement optimization problem

Without loss of generality, we consider a patch $\mathcal{P}_k = \{T_i\}_{i=1,\cdots,n_k}$ constructed around an invalid element T_k, where n_k refers to the number of elements in the patch. We cast the validity improvement of the patch elements as a constrained optimization problem :

$$\begin{array}{ll} \min\limits_{\mathbf{x},s} & s \\ \textit{s.t.} & \\ & \forall T_i \in \mathcal{P}_k \begin{cases} \underbrace{-\mathbf{n}\cdot\det(\vec{a}_{16},\vec{a}_{26})}_{g_1} & \leq \; s \\ \underbrace{-\mathbf{n}\cdot\det(\vec{a}_{24},\vec{a}_{34})}_{g_2} & \leq \; s \\ \underbrace{-\mathbf{n}\cdot\det(\vec{a}_{56},\vec{a}_{54})}_{g_3} & \leq \; s \\ \underbrace{-\mathbf{n}\cdot(\det(\vec{a}_{16},\vec{a}_{34})+\det(\vec{a}_{24},\vec{a}_{26}))}_{g_4} & \leq \; s \\ \underbrace{-\mathbf{n}\cdot(\det(\vec{a}_{54},\vec{a}_{16})+\det(\vec{a}_{26},\vec{a}_{56}))}_{g_5} & \leq \; s \\ \underbrace{-\mathbf{n}\cdot(\det(\vec{a}_{54},\vec{a}_{24})+\det(\vec{a}_{34},\vec{a}_{56}))}_{g_6} & \leq \; s \end{cases} \end{array} \tag{6}$$

where **x** denotes the coordinates vector of the free nodes and control points in the patch $\mathcal{P}_k$, **n** the normal vector to the surface element $T_i \in \mathcal{P}_k$ and s an additional variable that is expressed in terms of the most restricting validity constraints :

$$s > \max_{j=1,\cdots,6} g_j^k.$$

This variable can thus be viewed as the maximum infeasibility of the jacobian positivity constraints. The idea will thus be to minimize the latter variable and drive it below zero.

The local minimization problem is then rewritten as an unconstrained optimization one using the log-barrier method :

$$\min_{\mathbf{x},s} \mathcal{F}(s,\mathbf{x},t) \tag{7}$$

with,

$$\mathcal{F}(s,\mathbf{x},t) = s - \frac{1}{t}\sum_{\forall T_i \in \mathcal{P}_k}\sum_{j=1}^{6}\log(s - g_j^{T_i}(\mathbf{x})) \tag{8}$$

where $t > 0$ is a scalar that calibrates the accuracy of the problem.

Since the developed approach will only be applied to untangle elements on the surface of the domain, then the mesh nodes and control points will be constrained to move in a geometry preserving way. Consequently, the variables will no longer be the cartesian coordinates of the points but the parametric coordinates (u, v) of the points on the surface and their movement will be dictated by the Bézier surface formula (eq. (9)) describing the geometry's surface. Furthermore, the points that belong to a domain ridge can only slide along that ridge and hence a single variable w is associated to them and the movement is dictated by the Bézier curve formula (eq. (10)).

$$\begin{aligned}\mathcal{S}(u,v) &= u^2P_1 + 2uvP_2 + v^2P_3 + v(1-u-v)P_4 \\ &\quad +2(1-u-v)^2P_5 + 2u(1-u-v)P_6 \end{aligned} \tag{9}$$

$$\mathcal{B}(w) = (1-w)^2P_1 + 2w(1-w)P_2 + w^2P_3 \tag{10}$$

The functional gradient will therefore be expressed in terms of the new variables :

$$\nabla\mathcal{F}(s,u,v,w,t) := \begin{cases} \frac{\partial\mathcal{F}(s,u,v,w,t)}{\partial u} = \frac{\partial\mathcal{F}(s,u,v,w,t)}{\partial\mathbf{x}}\frac{\partial\mathbf{x}}{\partial u} & \textit{for surface nodes} \\ \frac{\partial\mathcal{F}(s,u,v,w,t)}{\partial v} = \frac{\partial\mathcal{F}(s,u,v,w,t)}{\partial\mathbf{x}}\frac{\partial\mathbf{x}}{\partial v} & \textit{for surface nodes} \\ \frac{\partial\mathcal{F}(s,u,v,w,t)}{\partial w} = \frac{\partial\mathcal{F}(s,u,v,w,t)}{\partial\mathbf{x}}\frac{\partial\mathbf{x}}{\partial w} & \textit{for ridge nodes} \\ \frac{d\mathcal{F}(s,u,v,w,t)}{ds} & \textit{for the variable } s \end{cases} \tag{11}$$

where $\left(\frac{\partial\mathbf{x}}{\partial u}, \frac{\partial\mathbf{x}}{\partial v}\right)$ and $\frac{\partial\mathbf{x}}{\partial w}$ represent respectively the tangent plane and tangent vector to the surface at the point **x**. These tangents can either be determined from the CAD model or computed using the Bézier formula representing each of the elements under investigation as illustrated in equations (12), (13) and (14). In here, $\mathcal{S}(u,v)$ stands for the Bézier surface representing an element with its vertices $P_1,\ P_3,\ P_5$ and control points $P_2,\ P_4,\ P_6$ and $\mathcal{B}(w)$ the parametric Bézier curve reflecting a ridge of the domain.

$$\begin{aligned}\frac{\partial\mathbf{x}}{\partial u} &= \mathcal{S}_u(u,v) \\ &= 2uP_1 + 2vP_2 - 2vP_4 - 2(1-u-v)P_5 + 2(1-2u-v)P_6 \end{aligned} \tag{12}$$

$$\begin{aligned}\frac{\partial\mathbf{x}}{\partial v} &= \mathcal{S}_v(u,v) \\ &= 2vP_3 + 2uP_2 - 2uP_6 - 2(1-u-v)P_5 + 2(1-2v-u)P_2 \end{aligned} \tag{13}$$

$$\begin{aligned}\frac{\partial\mathbf{x}}{\partial w} &= \mathcal{B}'(w) \\ &= -2(1-w)P_1 + 2(1-2w)P_2 + 2wP_3 \end{aligned} \tag{14}$$

The log-barrier problem is then iteratively solved using a conjugate gradient approach whereby the function is minimized along the direction of its gradient which points onto the improvement of the validity of each of the elements in the patch with a higher weight given to the elements whose mapping jacobian is negative. Consequently at each iteration of the iterative minimization, the nodes and control points are simultaneously re-positioned to lower the maximum infeasibility of the constraints. The algorithm comprises two phases : an outer phase whereby the value of t is increased iteratively and s is updated to

the new most restrictive validity constraint and an inner phase where the functional $\mathcal{F}(s, \mathbf{x}, t)$ is minimized using a conjugate gradient method. We note that the log-barrier method involves a backtracking line search process that determines the optimal movement along the gradient's direction.

It is important to mention that a patch can contain more than one invalid element. In that case, the local optimization algorithm will also treat the neighboring invalid element and improve its validity.

An example showing the applicability of the method even with very limited number of elements is shown in figure 4. On the left, the mesh is represented before untangling ; we can see along the internal boundary the invalid elements (presenting crossing edges). A single iteration of the local topological optimization approach was sufficient to obtain the valid mesh with curved elements.

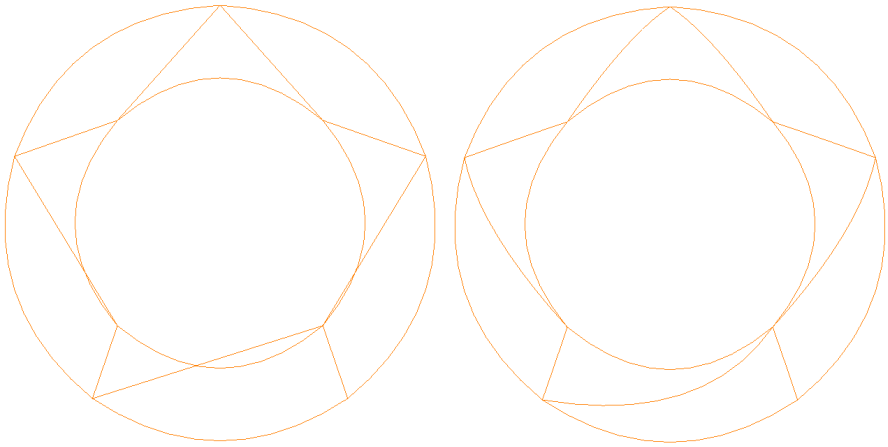

FIGURE 4 – Invalid ring mesh with curved boundaries (left) and untangled valid mesh (right).

As mentioned earlier, the mesh untangling procedure will only be applied to render valid triangles on the surface of the $3D$ domain. The method will therefore be coupled with another approach based on a linear elasticity analogy in the view of generating a valid starting mesh. The latter approach was introduced in [5] and will be outlined in the following section.

5 Volume untangling procedure via linear elasticity analogy

The main objective of the volume untangling procedure is to propagate the boundary curvature into the volume mesh. We note that at this stage, the surface mesh has valid triangles. The problem will be addressed by working on a subdivided mesh in which the vertices are considered as the control points of the curved mesh. Properties 2.1 and 2.2 imply that the validity of the subdivided mesh induces the validity of the associated curved mesh. The main advantage to consider this subdivided mesh relies in the exclusive focus on linear elements whose volume is very easily computed and consequently the validity evaluation can be directly deduced. The second advantage of considering subdivided meshes is a numerical one related to the ease of applying the linear elasticity solver on $\mathcal{P}_1$ finite elements, instead of applying it to $\mathcal{P}_2$ elements, quadratic Bézier. It is computationally much cheaper and yields a better control on the individual behaviors of the control points. This is obtained by considering the control points of the elements in the mesh. The mesh will then be subdivided and deformed (fig. 5).

On the curved boundary, we impose that the control points that define the boundary are exactly recovered. A linear elasticity analogy will then be adopted in order to generate the aimed valid mesh.
The initial mesh, $\mathcal{T}_0^h$, is treated as an elastic material with Lamé coefficients. It is then deformed and a

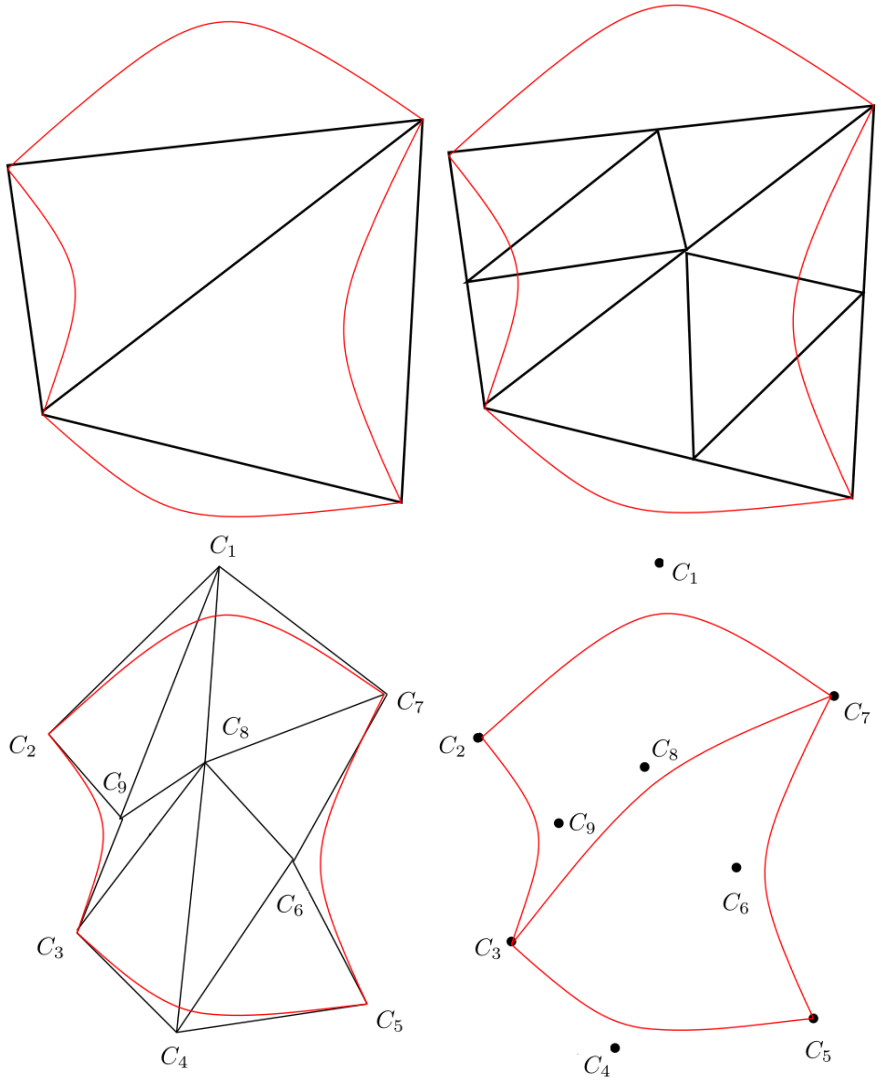

FIGURE 5 – Steps of the subdivided mesh generation algorithm : from an initial linear mesh (top-left) we subdivide the elements (top-right), then we deform the boundary elements so that the control points match exactly the curved domain's boundary (bottom-left) and finally we generate the deformed internal mesh using the control points of the subdivided mesh (bottom-right). *N.B :* the boundary of Ω (red) is parametrized by quadratic Bézier curves.

new mesh, $\mathcal{T}_D^h$, is obtained by solving the linear elasticity problem (15), so that the discrete boundary fits exactly the curved domain's boundary.

$$\begin{cases} \text{div}\left(\lambda \text{tr}(\nabla u)\mathbb{I} + \mu(\nabla u + \nabla u^T)\right) = 0 & \text{on } \Omega \\ u = g & \text{on } \partial\Omega. \end{cases} \tag{15}$$

where $\lambda > 0$ and $\mu > 0$ are the Lamé coefficients and $\mathbb{I}$ is the identity matrix. The imposed boundary condition is defined in such a way that a deformed element $K^D \in \mathcal{T}_D^h$ has the same orientation as the

initial mesh $K^0 \in \mathcal{T}_0^h$. This is achieved by preventing the volume of the element from changing its sign. We consider the mapping :

$$\omega_{K^0} : \theta \mapsto \text{Vol}\Big(\text{convex}(A^0_{i_1} + \theta u(A^0_{i_1}), \ldots, A^0_{i_{d+1}} + \theta u(A^0_{i_{d+1}}))\Big),$$

then $\omega_{K^0}(0) = \text{Vol}(K^0) > 0$. Thus, the problem reduces to finding the smallest θ such that $\omega_{K^0}(\theta) = 0$. This is achieved by solving for the smallest root of a quadratic (in 2D) or a cubic (in 3D) polynomial on all the simplexes of $\mathcal{T}^0$.

Nevertheless, an additional constraint should be imposed to prevent zero-volume elements : $\omega_{K^0}(\theta) > \lambda\, \omega_{min}$, where λ is a constant that we set to 0.9 in the numerical examples.

The interested reader is referred to [5] for further details on the choice of the boundary condition and the algorithm dedicated to its computation.

6 Numerical examples

We provide in this section some numerical examples to show the performance of the developed hybrid approach in untangling complex two and three dimensional geometries. We start by validating the surface untangling procedure via local topological optimization on two-dimensional problems. Then, we couple it with the volume untangling approach via linear elasticity and show their ability to generate a valid 3d curved mesh. We note that in all the examples, we have generated the initial curved meshes using the **GMSH** [11] and the **MMG3D** [12] meshing tools.

6.1 Multi-element airfoil

As a start, we consider the NASA 30p30n multi-element high-lift airfoil geometries and generate an initial mesh with curved elements that fit well the curvatures of the considered shapes. To make the test case more interesting, we have added boundary layers to the mesh. The bounding box of the domain is defined to $[-4615.2, 5384.8] \times [-4985.3, 5014.7]$. The initial mesh (fig. 6(left)), is made up from $5,008$ elements of which 79 are invalid. We can detect the highly stretched elements along the wing. Close-up views on the central wing (figures 6(center) and 7(left)) clearly show that the elements at the curved boundary are invalid and cross several elements in the boundary layer. The untangling procedure based on the local optimization approach was applied on this mesh and the resulting valid mesh is depicted, on the same closeup views, in figures 6(right) and 7(right). Only one iteration of the optimization algorithm was needed to get the final mesh. We can observe how the boundary layer structure was conserved by the untangling process ; this is a direct result of the local aspect of the method as the nodes and control points cannot move outside the local patch around the invalid element under consideration. We recall that since the method tends to improve the elements' validity criteria within the patch, several invalid element present in the patch can get untangled in a single shot hence accelerating the untangling process.

6.2 Mechanical part

As a second validation of the developed algorithm, we consider the geometry of a complex $3D$ mechanical part presenting several curvatures intersecting with sharp planar surfaces. The initial mesh (fig. 8), made up from $11,834$ tetrahedral elements and $18,261$ nodes, contains 34 invalid surface elements (of which 4 are on curved surfaces) and 266 invalid volume elements. Different snapshots of the mesh before (left) and after (right) untangling are depicted in figure 9. Three iterations of the local topological optimization method were employed to untangle the surface of the geometry and two iterations of the linear elasticity procedure were needed to render a valid curved mesh.

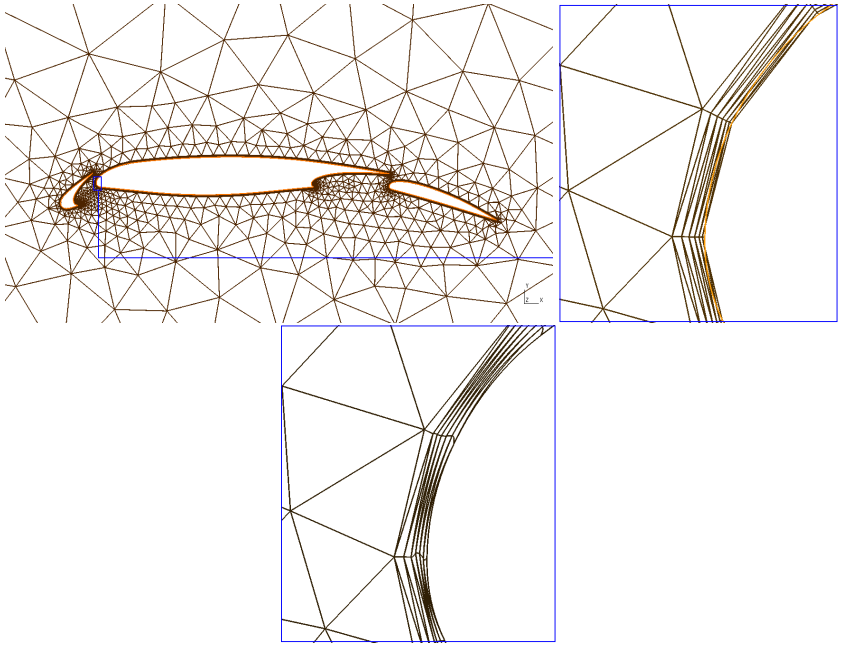

FIGURE 6 – Untangling of a multi-element airfoil. Initial mesh (left) zoom on the central wing with curved boundary (center) zoom on the untangled mesh (right).

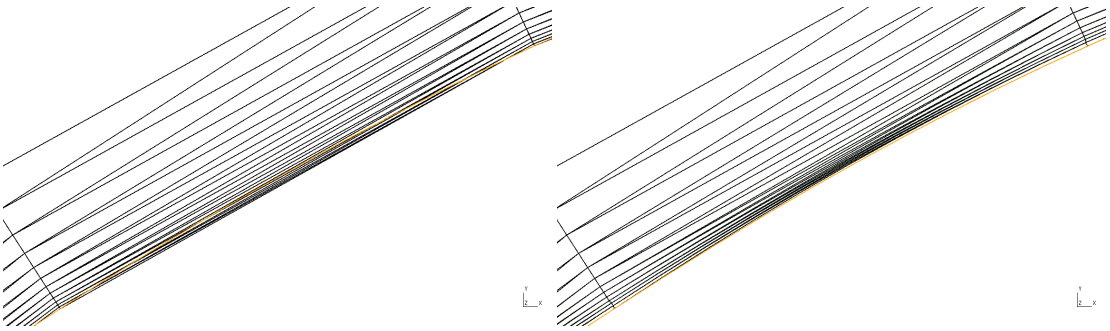

FIGURE 7 – Untangling of an element intersecting several elements in a boundary layer.

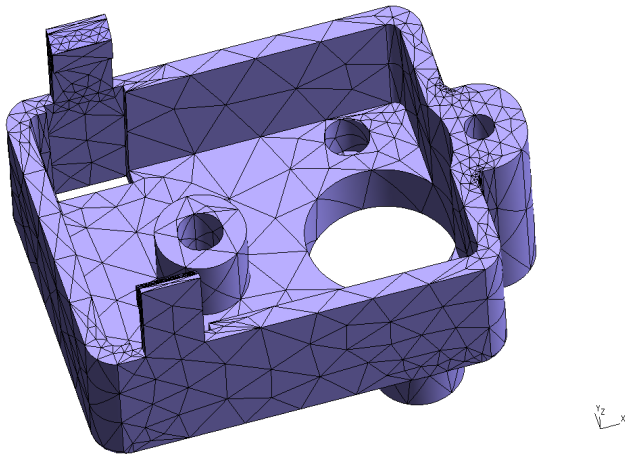

FIGURE 8 – Initial high order mesh of a mechanical part.

6.3 Airplane

For this example, we consider the geometry of a half of an airplane inside a half spherical domain. We designed the domain in such a way that is radius would be equal to forty times the length of the airplane. A zoom on the initial curved mesh around the airplane is represented on the figure 10. This initial mesh contains 134, 701 nodes and 759, 221 tetrahedra.

The curved mesh generation algorithm generated 24 invalid triangles in this initial curved mesh, in particular near the reactor (see figure 11(left)). Only one iteration of the optimization algorithm was needed to obtain a valid surface (see figure 11(right)). Following the surface mesh untangling process, the volume untangling was applied in order to render a valid volume mesh. A single iteration of elasticity was needed to untangle the three invalid tetrahedra present in the mesh.

6.4 M6 wing with boundary layers

We consider a M6 wing meshed with boundary layers. The first layer was built at a distance of $1e-4$ from the wing (see figure 12). The initial curved mesh has 26 invalid triangles mainly due to the boundary layers on the symetric plane (see figure 13). Three iterations of the optimisation algorithm were needed to obtain a valid surface while respecting the boundary layer structure. On the other hand, the mesh contained more than a hundred of invalid element. A single iteration of the linear elasticity algorithm was enough to untangle them.

7 Conclusions

In this paper, we have proposed a new method for generating valid high order meshes. The developed algorithm introduces a hybrid approach whereby the surface elements in a three-dimensional domain are untangled using a local topological optimization approach and the volume elements are treated using a linear elasticity analogy. The numerical results reflected the robustness in untangling invalid elements, the consistency in conserving the validity of existing valid elements and the efficiency of the mesh generation technique due to the local topological optimization around the invalid element. Finally, the method is automatic and does not require user interference. Different extensions of this work are planned on the

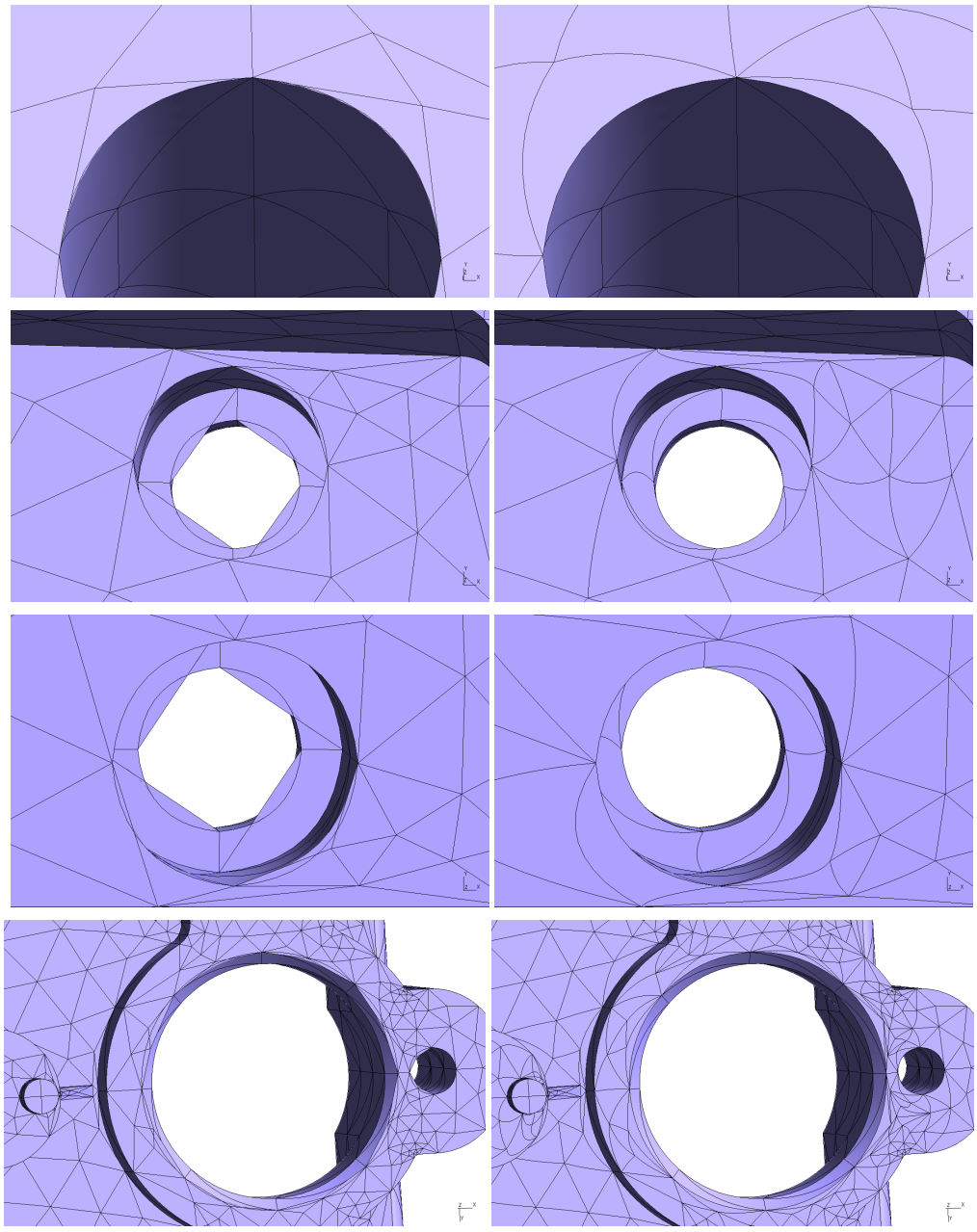

FIGURE 9 – Snapshots of the surface view at different positions of the mechanical part before (left) and after (right) untangling.

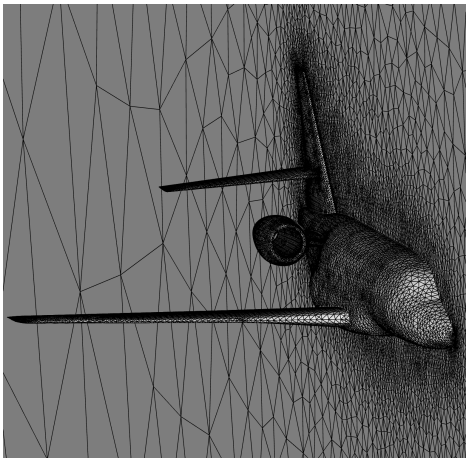

FIGURE 10 – Initial high order mesh of an airplane.

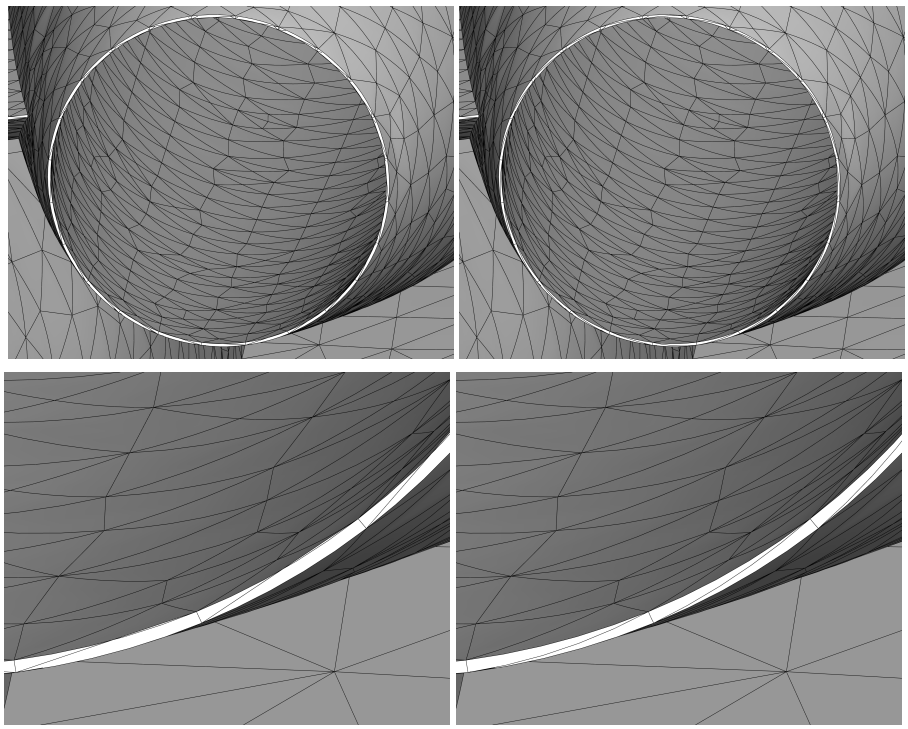

FIGURE 11 – Snapshots of the surface view near the reactor before (left) and after (right) untangling.

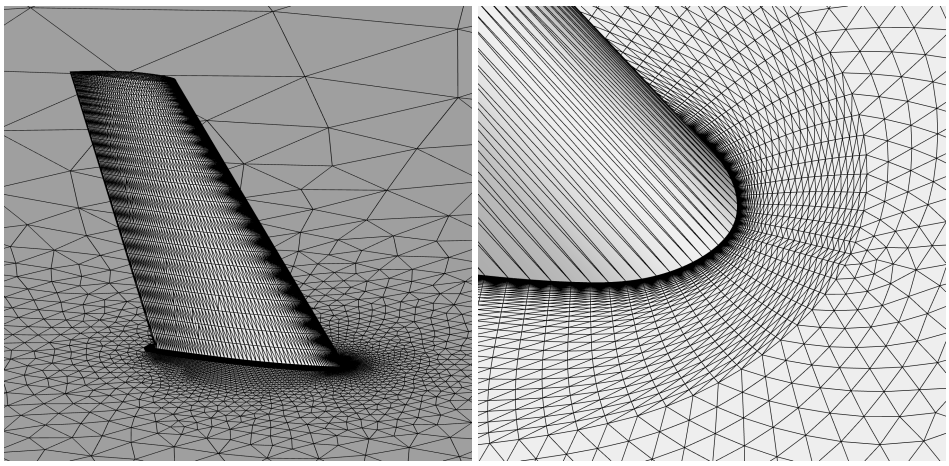

FIGURE 12 – Zoom on initial high order mesh of a M6 wing.

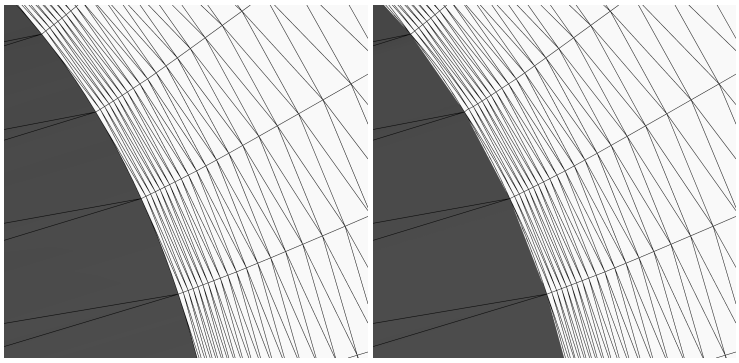

FIGURE 13 – Snapshots of the surface view before (left) and after (right) untangling.

high order meshing roadmap. On the one hand, we intend to account for both geometrical and physical anisotropies by adding a directional privilege for untangling. On the other hand, we intend to study the influence of the curved elements on the accuracy and convergence of the numerical scheme.

Acknowledgements.

G. Jannoun has been fully supported by the MAIDESC ANR project which is supported by the french ministery of Research under contract ANR-13-MONU-0010.

Experiments presented in this paper were carried out using the PLAFRIM experimental platform, being developed under the Inria PlaFRIM development action with support from Bordeaux INP, LABRI and IMB and other entities : Conseil Régional d'Aquitaine, Université de Bordeaux and CNRS (and ANR in accordance to the programme d'investissements d'Avenir (see http ://www.plafrim.fr/).

Références

[1] M. Shephard, J. Flaherty, K. Jansen, X. Li, X. Luo, N. Chevaugeon, J.-F. Remacle, M. Beall, and R. O'Bara, "Adaptive mesh generation for curved domains," *Applied Numerical Mathematics*, vol. 52, no. 2-3, pp. 251 – 271, 2005. Conference on Adaptive Methods for Partial Differential Equations and Large-Scale Computation.

[2] O. Sahni, X. Luo, K. Jansen, and M. Shephard, "Curved boundary layer meshing for adaptive viscous flow simulations," *Finite Elements in Analysis and Design*, vol. 46, no. 1-2, pp. 132 – 139, 2010. Mesh Generation - Applications and Adaptation.

[3] S. Dey, R. O'Bara, and M. Shephard, "Towards curvilinear meshing in 3d : the case of quadratic simplices," *Computer-Aided Design*, vol. 33, no. 3, pp. 199 – 209, 2001.

[4] S. Dey, R. O'Bara, and M. Shephard, "Curvilinear mesh generation in 3d," in *In proceedings of the eighth international meshing roundtable*, pp. 407–417, John Wiley & Sons, 1999.

[5] R. Abgrall, C. Dobrzynski, and A. Froehly, "A method for computing curved meshes via the linear elasticity analogy, application to fluid dynamics problems," *International Journal for Numerical Methods in Fluids*, vol. 76, no. 4, pp. 246–266, 2014.

[6] P. George and H. Borouchaki, "Construction of tetrahedral meshes of degree two," *International Journal for Numerical Methods in Engineering*, vol. 90, no. 9, pp. 1156–1182, 2012.

[7] Z. Xie, R. Sevilla, O. Hassan, and K. Morgan, "The generation of arbitrary order curved meshes for 3d finite element analysis," *Computational Mechanics*, vol. 51, no. 3, pp. 361–374, 2012.

[8] P. Persson and J. Peraire, "Curved mesh generation and mesh refinement using lagrangian solid mechanics," *47th AIAA Aerospace Sciences Meeting including The New Horizons Forum and Aerospace Exposition, Aerospace Sciences Meetings, Orlando, FL*, pp. 209–949, 2009.

[9] T. Toulorge, C. Geuzaine, J.-F. Remacle, and J. Lambrechts, "Robust untangling of curvilinear meshes," *Journal of Computational Physics*, vol. 254, pp. 8 – 26, 2013.

[10] J. P. J. S. A. Gargallo-Peiró, X. Roca, "High-order mesh generation on cad geometries," in *J.P.M. de Almeida, P. Díez, C. Tiago, N. Parés (Eds.), Proceedings of the VI International Conference on Adaptive Modeling and Simulation (ADMOS 2013), International Center for Numerical Methods in Engineering (CIMNE), Barcelona, Spain*, 2013.

[11] C. Geuzaine and J.-F. Remacle, "Gmsh : A 3-d finite element mesh generator with built-in pre- and post-processing facilities," *International Journal for Numerical Methods in Engineering*, vol. 79, no. 11, pp. 1309–1331, 2009.

[12] C. Dapogny, C. Dobrzynski, and P. Frey, "Three-dimensional adaptive domain remeshing, implicit domain meshing, and applications to free and moving boundary problems," *J. Comput. Phys.*, vol. 262, pp. 358–378, 2014.

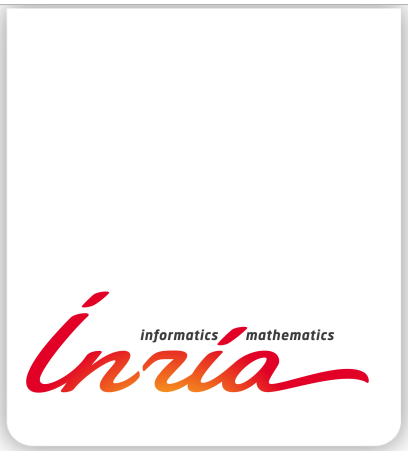

RESEARCH CENTRE
BORDEAUX – SUD-OUEST

200 avenue de la Vieille Tour
33405 Talence Cedex

Publisher
Inria
Domaine de Voluceau - Rocquencourt
BP 105 - 78153 Le Chesnay Cedex
inria.fr

ISSN 0249-6399